J. Fluid Mech. (2014), *vol.* 739, *pp.* 421–443.
doi:10.1017/jfm.2013.624

Lateral migration of a capsule in plane shear near a wall

Rajesh Kumar Singh[1,2], Xiaoyi Li[1,‡] and Kausik Sarkar[1,2,3,†]

[1]Department of Mechanical Engineering, University of Delaware, Newark, DE 19716, USA

[2]Biomechanics and Movement Science Program, University of Delaware, Newark, DE 19716, USA

[3]Department of Mechanical and Aerospace Engineering, George Washington University, Washington, DC 20052, USA

(Received 26 April 2013; revised 13 September 2013; accepted 19 November 2013)

The migration of a capsule enclosed by an elastic membrane in a wall-bounded linear shear is investigated using a front-tracking method. A detailed comparison with the migration of a viscous drop is presented varying the capillary number (in the case of a capsule, the elastic capillary number) and the viscosity ratio. In both cases, the deformation breaks the flow reversal symmetry and makes them migrate away from the wall. They quickly go through a transient evolution to eventually reach a quasi-steady state where the dynamics becomes independent of the initial position and only depends on the wall distance. Previous analytical theories predicted that for a viscous drop, in the quasi-steady state, the migration and slip velocities scale approximately with the square of the inverse of the drop–wall separation, whereas the drop deformation scales as the inverse cube of the separation. These power law relations are shown to hold for a capsule as well. The deformation and inclination angle of the capsule and the drop at the same wall separation show a crossover in their variation with the capillary number: the capsule shows a steeper variation than that of the drop for smaller capillary numbers and slower variation than the drop for larger capillary numbers. Using the Green's function of Stokes flow, a semi-analytic theory is presented to show that the far-field stresslet that causes the migration has two distinct contributions from the interfacial stresses and the viscosity ratio, with competing effects between the two defining the dynamics. It predicts the scaling of the migration velocity with the capsule–wall separation, however, matching with the simulated result very well only away from the wall. A phenomenological correlation for the migration velocity as a function of elastic capillary number, wall distance and viscosity ratio is developed using the simulation results. The effects of different membrane hyperelastic constitutive equations – neo-Hookean, Evans–Skalak, and Skalak – are briefly investigated to show that the behaviour remains similar for different equations.

Key words: biological fluid dynamics, capsule/cell dynamics, drops and bubbles

† Email address for correspondence: sarkar@gwu.edu

‡ Present address: United Technologies Research Center, East Hartford, CT 06108, USA.

1. Introduction

The deformation-induced migration of drops, capsules and cells plays a key role in structures and functions of many chemical and biological emulsions/suspensions. In blood flow, for example, migration of red blood cells (RBCs) away from the vessel wall creates a cell-depleted layer and reduces the overall viscosity (Fåhraeus 1929; Barbee & Cokelet 1971; Reinke, Gaehtgens & Johnson 1987). On the other hand, relatively less deformable cells – platelets and white blood cells – are expelled towards the vessel wall (Tangelder *et al.* 1985). Variation in deformability changes the lateral force on these cells, affecting their ability to adhere to the vessel wall under different physiological conditions (Damiano *et al.* 1996). Here, we investigate the migration of a capsule enclosed by an elastic membrane in simple shear near a wall.

The lateral migration of deformable particles away from a wall has a purely viscous origin (Leal 1980), and is absent for a rigid sphere in a wall-bounded plane shear. At zero Reynolds number without the influence of inertia, reversibility of the linear Stokes flow precludes lateral migration of rigid spheres. Deformation breaks the reversibility and the deformed particle migrates away from the wall. This phenomenon has been extensively investigated for the case of a viscous drop with an interface where the normal stress jump is given by the interfacial tension. A number of analytical results have been developed (Chaffey, Brenner & Mason 1965; Karnis & Mason 1967; Chan & Leal 1979; Shapira & Haber 1990; Imaeda 2000) using perturbation theory. However, the theories are limited to small deformations and far from the wall, and they neglected alterations of deformation and orientation due to the presence of the wall. The results showed large discrepancies when compared with experiments (Karnis & Mason 1967). Improved predictions were achieved using boundary element simulations of large drop deformation (Uijttewaal, Nijhof & Heethaar 1993; Kennedy, Pozrikidis & Skalak 1994; Uijttewaal & Nijhof 1995). Smart & Leighton (1991), in an elegant presentation, elucidated that the wall-induced migration of a drop arises due to the stresslet field generated by the drop – more specifically by the flow induced by the image stresslet on the other side of the wall. Recently, we have shown that in a shear-induced pair-collision between two viscous drops in a confined shear, the wall-induced migration makes them organize at a specific separation in the centre of the domain (Sarkar & Singh 2013).

There have been fewer investigations of the lateral migration of more complex particles such as elastic capsules. Capsule shape in the small deformation limit has been analysed using perturbation theories (Barthes-Biesel 1980; Barthes-Biesel & Rallison 1981). Bagchi and co-workers, in a number of articles, applied an immersed boundary technique to study the behaviours of single (Doddi & Bagchi 2008; Bagchi & Kalluri 2009) and multiple neo-Hookean capsules (Doddi & Bagchi 2009) in a plane Poiseuille flow. There a balance between the wall effects and shear gradient effects determines the equilibrium positions of the capsules. A recent two-dimensional study (Coupier *et al.* 2008; Kaoui *et al.* 2008; Li & Ma 2010) showed that elastic capsules and vesicles (fluid bodies enclosed by an area-preserving membrane characterized by a bending resistance energy) migrate toward the centre of the Poiseuille flow, in contrast to a drop which moves to an off-centre position. Introduction of inertia plays an important role in determining the equilibrium positions (Shin & Sung 2011). There have also been a number of studies of the lift of a vesicle near a wall (Olla 1997*a*,*b*; Callens *et al.* 2008; Farutin & Misbah 2013), showing that the vesicle experiences a tank-treading (membrane rotation) motion with a steady tilt. Lift may also induce unbinding of a tank-treading vesicle adhered to a wall by non-specific interactions; the small clearance between the vesicle and the wall

allowed a lubrication analysis within the binding regions, which gave an estimation of the lift force (Cantat & Misbah 1999; Seifert 1999). Further quantitative experiments (Lorz *et al.* 2000; Abkarian & Viallat 2005) confirmed the existence of a lift force. More recently, boundary element simulation was used to show the formation of a cell depletion layer in a suspension of capsules in viscous and viscoelastic matrices (Pranay, Henriquez-Rivera & Graham 2012). In view of the majority of the above studies being in Poiseuille flow, we note that there the shear rate gradient plays a role in migration. In contrast, in simple shear characterized by a constant shear rate, the migration is exclusively caused by the presence of the wall, making it an interesting case in its own right.

Here, we use a front-tracking finite difference method to directly simulate the deformation and motion of a capsule enclosed by an elastic membrane near a wall in plane shear. The front-tracking method provides a comprehensive framework to study various complex effects including inertia (Sarkar & Schowalter 2001; Li & Sarkar 2005, 2006; Singh & Sarkar 2011), membrane/fluid viscoelasticity (Sarkar & Schowalter 2000; Li & Sarkar 2008; Aggarwal & Sarkar 2007, 2008*a*,*b*; Mukherjee & Sarkar 2009, 2010, 2011, 2013), and multi-particle interactions (Olapade, Singh & Sarkar 2009; Singh & Sarkar 2009; Sarkar & Singh 2013). This paper is organized as follows. In § 2, we briefly describe the mathematical formulation of the fluid flow and membrane forces. The numerical algorithm is described in § 3. In § 4, results on capsule deformation, orientation and migration velocity are presented. We discuss in detail the quasi-steady dynamics and its dependence on the capillary number and the instantaneous distance from the wall. We offer a detailed comparison between drop and capsule migration. Using a Green's function formulation of the Stokes flow around a drop or a capsule, we develop an approximate theory for the migration that explains the different scalings numerically observed. Using the simulated results, we provide a phenomenological correlation for the migration of an elastic capsule as a function of capillary number, capsule–wall separation and viscosity ratio. Finally, the effects of different constitutive equations are briefly considered. Results are summarized in § 5.

2. Governing equations

The mathematical formulation has been described in detail previously (Li & Sarkar 2008). Here it is only briefly sketched. The flow is governed by the continuity and Navier–Stokes equations:

$$\boldsymbol{\nabla}\cdot\boldsymbol{u}=0, \tag{2.1}$$

$$\frac{\partial(\rho\boldsymbol{u})}{\partial t}+\boldsymbol{\nabla}\cdot(\rho\boldsymbol{u}\boldsymbol{u})=-\boldsymbol{\nabla}p+\boldsymbol{\nabla}\cdot[\mu\{\boldsymbol{\nabla}\boldsymbol{u}+(\boldsymbol{\nabla}\boldsymbol{u})^{\mathrm{T}}\}]-\int_{\partial B}\boldsymbol{f}^{m}(\boldsymbol{x}')\delta(\boldsymbol{x}-\boldsymbol{x}')\,\mathrm{d}S(\boldsymbol{x}'), \tag{2.2}$$

where p is the pressure, ρ is the density and μ is the viscosity of the fluid. The density and viscosity are uniform in each phase and are allowed to have a sharp variation across the membrane ∂B separating them. In this work, the capsule is assumed to be neutrally buoyant with the same density as that of the liquid outside. The superscript $^{\mathrm{T}}$ represents the transpose; $\boldsymbol{f}^{m}$ is the elastic membrane forces arising as a jump in the stress condition across the membrane. The elastic stress in the membrane is determined by the initial membrane configuration and its deformation state via two-dimensional constitutive laws. In this paper, three different constitutive laws for membranes are considered: neo-Hookean, Skalak and Evans & Skalak (Barthes-Biesel, Diaz & Dhenin 2002; Evans & Skalak 1979; Skalak *et al.* 1973). Note that for a drop

the force at the interface is simply due to the interfacial tension σ_s (Singh & Sarkar 2011).

A neo-Hookean membrane (denoted by NH below) is an example of a class of models that assume the membrane to be an infinitely thin sheet of an isotropic volume-incompressible elastic medium. The area of the membrane is allowed to change, with the implicit assumption that it is balanced by the thinning of the membrane. Its strain-energy function is

$$W = \frac{G_s}{2}\left(\lambda_1^2 + \lambda_2^2 + \frac{1}{\lambda_1^2\lambda_2^2}\right), \tag{2.3}$$

where λ_1 and λ_2 are the principal stretches on the membrane surface. The principal membrane stresses are

$$\tau_1^m = \frac{1}{\lambda_2}\frac{\partial W}{\partial \lambda_1} = \frac{G_s}{\lambda_1\lambda_2}\left(\lambda_1^2 - \frac{1}{\lambda_1^2\lambda_2^2}\right), \tag{2.4a}$$

$$\tau_2^m = \frac{1}{\lambda_1}\frac{\partial W}{\partial \lambda_2} = \frac{G_s}{\lambda_1\lambda_2}\left(\lambda_2^2 - \frac{1}{\lambda_1^2\lambda_2^2}\right). \tag{2.4b}$$

Skalak *et al.* (1973) proposed a constitutive model for the red blood cell membrane (denoted by SK below), that incorporates area-incompressibility. The strain-energy function is given by

$$W = \frac{G_s}{4}[(\lambda_1^4 + \lambda_2^4 - 2\lambda_1^2 - 2\lambda_2^2 + 2) + C(\lambda_1^2\lambda_2^2 - 1)^2]. \tag{2.5}$$

A large value of C indicates approximate area-incompressibility. The principal membrane stresses are

$$\tau_1^m = \frac{G_s}{\lambda_1\lambda_2}\left[\lambda_1^2(\lambda_1^2 - 1) + C\lambda_1^2\lambda_2^2(\lambda_1^2\lambda_2^2 - 1)\right], \tag{2.6a}$$

$$\tau_2^m = \frac{G_s}{\lambda_1\lambda_2}\left[\lambda_2^2(\lambda_2^2 - 1) + C\lambda_1^2\lambda_2^2(\lambda_1^2\lambda_2^2 - 1)\right]. \tag{2.6b}$$

Evans & Skalak (1979) simplified the above constitutive model by adding linearly and independently contributions of the shear and dilations (denoted by ES). The modified strain energy function is

$$W = G_S\left[\left(\frac{\lambda_1^2 + \lambda_1^2}{2\lambda_1^2\lambda_2^2} - 1\right) + A(\lambda_1\lambda_1 - 1)^2\right]. \tag{2.7}$$

The area dilation modulus is simply proportional to the shear modulus ($K_s = AG_S$) and the principal membrane stresses are

$$\tau_1^m = G_S\left[\frac{1}{2\lambda_1^2\lambda_2^2}(\lambda_1^2 - \lambda_2^2) + A(\lambda_1\lambda_2 - 1)\right], \tag{2.8a}$$

$$\tau_2^m = G_S\left[\frac{1}{2\lambda_1^2\lambda_2^2}(\lambda_2^2 - \lambda_1^2) + A(\lambda_1\lambda_2 - 1)\right]. \tag{2.8b}$$

At $C = 1$ and $A = 3$, the NH, SK and ES models predict the same deformation of the membrane with ($K_s = 3G_S$) at a small deformation limit, but they show different nonlinear stress–strain relations for large deformation (Lefebvre & Barthes-Biesel 2007). From relative deformation, the principal directions $\boldsymbol{g}_1$, $\boldsymbol{g}_2$ and corresponding

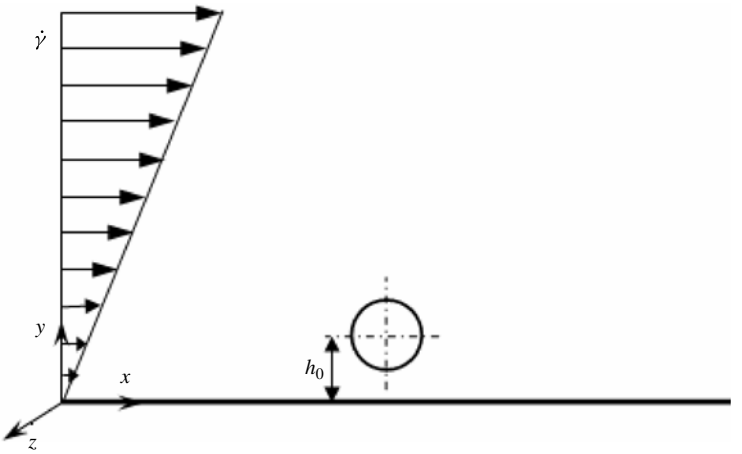

FIGURE 1. A schematic diagram of the flow of a capsule near a wall in a shear flow.

stretches are obtained. Equations (2.4), (2.6) or (2.8) are used to obtain the principal stresses. The stress tensor in an element is

$$\boldsymbol{\tau}^m = \tau_1^m \boldsymbol{g}_1 \otimes \boldsymbol{g}_1 + \tau_2^m \boldsymbol{g}_2 \otimes \boldsymbol{g}_2, \tag{2.9}$$

which can then be used to calculate the membrane force $\boldsymbol{f}^m$ in (2.1). In the present formulation, we do not consider stresses due to membrane bending.

3. Problem setup and numerical implementation

We investigate deformation and lateral migration of a capsule in simple shear near a wall. A spherical capsule with radius a is initially placed at a distance h_0 from the bottom wall (see figure 1). Simulations are performed in a rectangular computational domain of size $10a \times 10a \times 5a$ in the flow (x), gradient (y) and vorticity (z) directions respectively. Periodic boundary conditions are imposed in the flow and the vorticity directions. In the gradient direction, the bottom wall is at rest, and the top wall (assumed to be sufficiently far away from the bottom wall and the capsule) is moving with a velocity U to generate a shear rate $\dot{\gamma} = U/10a$. The effects of the top wall have been investigated to find that the capsule dynamics remain independent until the capsule reaches a distance from the bottom wall $h/a > 3.5$.

The governing equation (2.1) is solved in a three-dimensional staggered (volume) grid. The capsule membrane is described by the interface (front) separately discretized by a triangular mesh (Sarkar & Schowalter 2001; Tryggvason *et al.* 2001; Li & Sarkar 2005). The membrane force is computed using the deformation of the triangular element on the front from its initial undeformed configuration (Eggleton & Popel 1998; Shrivastava & Tang 1993). During deformation, each element remains flat and the strain is homogeneous within each element. Principal strains computed from the deformation are used in (2.4), (2.6) or (2.8) along with (2.9) to obtain the stresses at each element. The forces along the element edges were computed and the total force exerted on each membrane node is computed by adding the elastic forces acting on all the element edges connected to that node. A fractional-step projection algorithm is

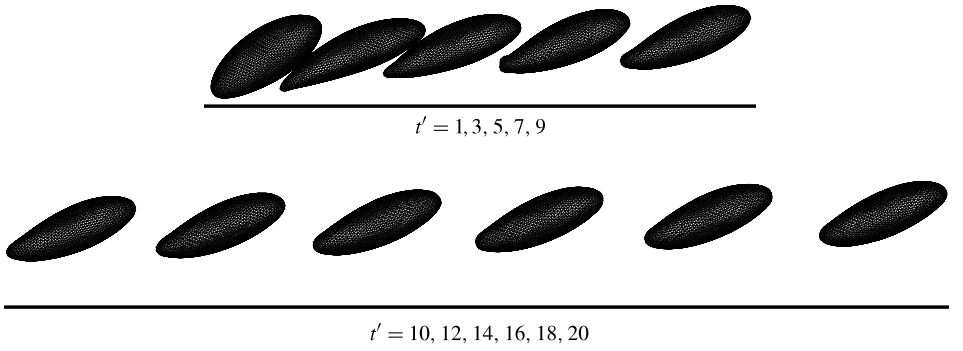

FIGURE 2. Initial shapes of the capsule during the migration. It first becomes asymmetric and then migrates away from the wall: $h_0/a = 1.2$, $\varepsilon = 0.6$ and $\lambda = 1$. The solid line indicates the wall.

used to solve the problem. The pressure Poisson equation is solved using a multi-grid method. An ADI scheme is applied for the viscous terms to alleviate the severe diffusion limited restriction ($\Delta t < 0.25(\Delta x)^2\rho/\mu$) on time steps.

We use a uniform $96 \times 96 \times 48$ grid in the computational domain and a surface mesh with 10 242 nodes for tracking the membrane, unless otherwise specified. The ratio of an element edge to the grid spacing is 0.66 for the initial undeformed configuration so that appropriate grid-front property transfer is ensured. The numerical convergence of the simulation tool was presented in a previous publication (Li & Sarkar 2008). The problem is governed by dimensionless parameters $\varepsilon = \mu_m a\dot{\gamma}/G_s$ (elastic capillary number) and $\lambda = \mu_d/\mu_m$ (viscosity ratio), and h/a (normalized capsule–wall distance). In the case of drops, the elastic capillary number is replaced by $Ca = \mu_m a\dot{\gamma}/\sigma_s$. The explicit nature of the algorithm restricts simulation at $Re = 0.05$ to approximate Stokes flow simulation.

4. Results and discussion

4.1. *Transient deformation and migration*

First we consider a capsule enclosed by a neo-Hookean (NH) membrane ($\varepsilon = 0.6$, $\lambda = 1$) placed initially at $h_0 = 1.2a$. Figure 2 shows its evolving shape as it moves away from the wall at various $t' = \dot{\gamma}t$. Initially (see e.g. $t' = 1.0$) the capsule deforms into an ellipsoid with a symmetric shape, showing negligible effects of the wall. After $t' = 3$, further deformation breaks the symmetry in shape due to the wall: a higher deformation of the capsule results in a tail shape near the wall. Due to the membrane compressive force, the tail has a tendency to retract. Similar asymmetric shapes were also observed for a viscous drop in shear near a wall (Uijttewaal *et al.* 1993). The deformed capsule moves in the flow direction and simultaneously moves away from the wall. As the distance between the capsule and the wall increases, the influence of the wall decreases. Owing to the reduced wall effect, the stress relaxes, the tail gradually disappears, and eventually the capsule gains an approximately ellipsoidal shape. At $t' = 50$, the capsule reaches $h/a \approx 3.0$, where wall effects on the shape seem to be negligible, the shape now being almost symmetric.

We define the axes of the capsule using an inertia tensor:

$$\boldsymbol{I}^d = \int_V (r^2\boldsymbol{I} - \boldsymbol{xx})\,\mathrm{d}^3r = \frac{1}{5}\int_{\partial V} (r^2\boldsymbol{xI} - \boldsymbol{xxx})\cdot\boldsymbol{n}\,\mathrm{d}^2r, \tag{4.1}$$

where $\boldsymbol{I}$ is the identity tensor. The relations between the eigenvalues $I^d_{L,B,W}$ of $\boldsymbol{I}^d$ and the major axes of the capsule are

$$L = \sqrt{\frac{5}{2\rho V}(I^d_B + I^d_W - I^d_L)}, \tag{4.2}$$

$$B = \sqrt{\frac{5}{2\rho V}(I^d_L + I^d_W - I^d_B)}, \tag{4.3}$$

$$W = \sqrt{\frac{5}{2\rho V}(I^d_L + I^d_B - I^d_W)}. \tag{4.4}$$

We compare the cases in the presence and absence of the wall in figure 3(*a*) by plotting the transient deformation $D = (L-B)/(L+B)$ and the orientation angle φ (the angle between the largest axis L and the flow direction). In the initial stage before $t' \simeq 1.0$, D and φ are identical in the presence and absence of the wall. Afterwards, the capsule in the presence of the wall becomes more aligned with the flow and φ shows a slight undershoot. After $t' \simeq 15$, the capsule is sufficiently far from the wall that the effects of wall on φ become negligible. After the initial stage and before the capsule migrates far from the wall, D shows a large increase from the no-wall case primarily due to increased L (not shown here for the reasons of brevity). In the long time limit, deformation curves for both cases gradually converge.

The wall-induced migration is depicted in the inset of figure 3(*b*) by the evolution of the x and y coordinates of the centre of mass of the capsule. The capsule moves in the flow direction shown by x_c increasing with time. In the initial stage before $t' \simeq 1.0$, y_c remains close to $1.2a$ and the capsule hardly moves in the lateral direction (figure 1). After $t' \geqslant 3$, as the shape loses its symmetry, the capsule starts moving in the lateral direction. Corresponding velocities are also shown in figure 3(*b*). We compute the slip velocity – the relative velocity between the unperturbed fluid and the capsule $V_{slip} = \dot{\gamma}h - V_x$ ($\dot{\gamma}h$ is the unperturbed velocity at the capsule's centre of mass and V_x is the streamwise velocity of the capsule's centre). Migration and slip velocities of the capsule are non-dimensionalized by $\dot{\gamma}a$. Both velocities remain small before $t' \simeq 1.0$. Then they quickly increase to a maximum due to excess deformation. Subsequently, both velocities slowly decrease as a result of increasing capsule–wall distance. Similar to the case of a drop subjected to shear (Uijttewaal *et al.* 1993), migration velocities are highly dependent on the deformation. The slip velocity is almost twice the value of the migration velocity and its positive value shows the capsule lagging behind the flow.

In figure 4, we plot the migration velocity of the capsule as a function of the capsule–wall distance (h/a) with different starting positions h_0/a. The inset plots the corresponding deformation. Note that after transient lateral displacement, the capsule adapts itself to the flow and reaches a quasi-steady state, where the deformation and the migration velocity become independent of the initial position. They are then only functions of the instantaneous lateral position of the centre of the capsule from the wall (h/a). In the following, we discuss the behaviour of a capsule that has reached a quasi-steady state.

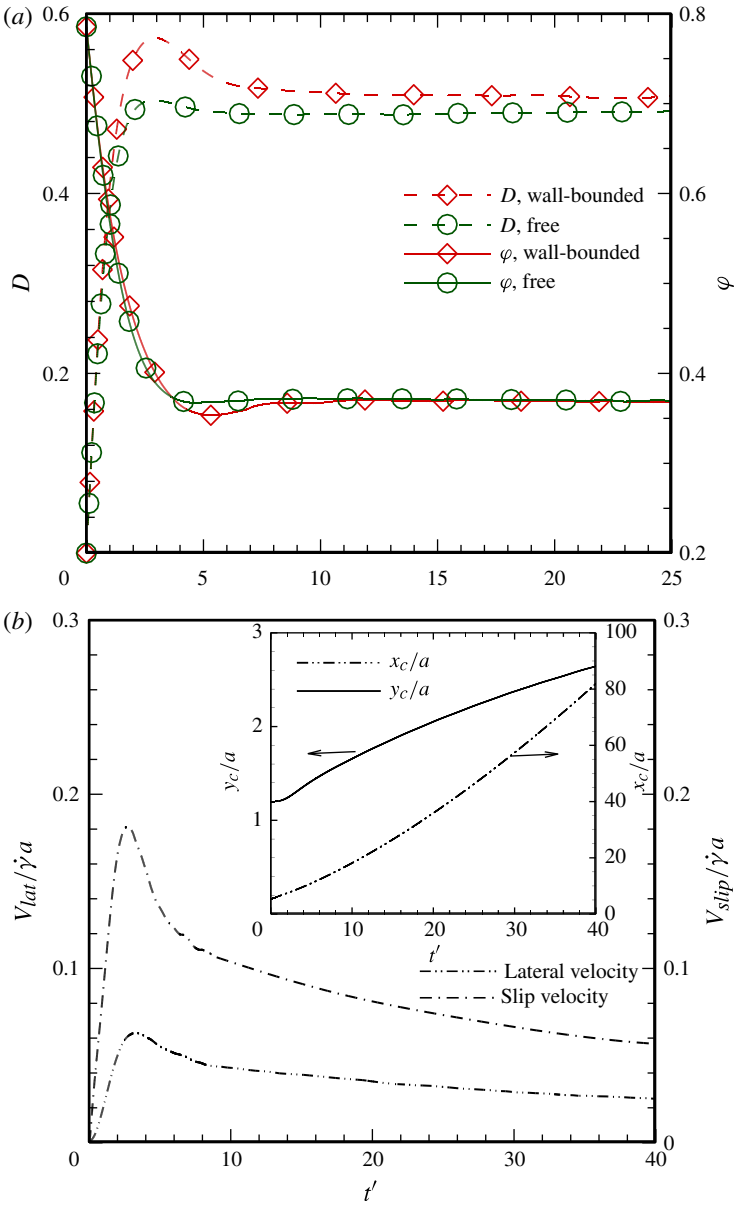

FIGURE 3. (Colour online) (*a*) Temporal evolution of the deformation D and orientation angle φ of a neo-Hookean capsule at $\varepsilon = 0.60$ and $\lambda = 1$. The results for free and wall-bounded conditions are compared. (*b*) Lateral and slip velocities with time. The inset of (*b*) shows the temporal evolution of the x and y coordinates of the centre of the capsule.

4.2. *Effects of capillary number in quasi-steady state and comparison with drops*

Due to the development of compressive stresses in an elastic membrane (Lac *et al.* 2004), the capsule shape may become unstable in the absence of bending resistance leading to surface buckling. The formation of such buckles in an unbounded shear at low capillary numbers (ε) has been previously investigated and discussed

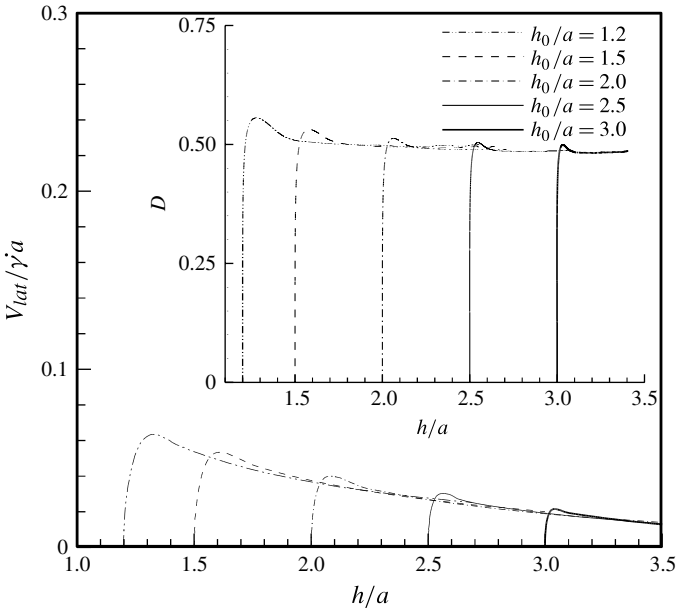

FIGURE 4. Evolution of the lateral velocity of an NH capsule starting at different initial positions with $\varepsilon = 0.6$ and $\lambda = 1$. The inset shows the evolution of deformation for the same case.

(Li & Sarkar 2008). There we found that the numerical buckling instability is somewhat alleviated due to the smoothing involved in the front-tracking algorithm. At low ε, even when a capsule tends to be unstable, it can always reach a quasi-steady D and φ before buckling instability sets in. Here, we do not explore the capsule behaviour beyond the unstable point. In figure 5(*a*), we plot the quasi-steady deformation and orientation angle as functions of capillary number ε at different capsule–wall distances, h/a. Different cases reach a value of h/a at different time instants. Increasing ε decreases elastic stresses in the membrane compared to deforming viscous stresses. Therefore, for a fixed value of h/a, D increases with increasing ε. The orientation angle decreases with increasing ε; similar to a drop, the more elongated the capsule is, the more it aligns with the flow. The decrease of capsule–wall distance h/a leads to a slight increase in D but negligible change in φ. Note that D is less sensitive to h/a at larger values of h/a.

In addition to deformation, a spherical capsule also exhibits a tank-treading motion: a fluid particle on the membrane goes around the capsule due to the vorticity in the shear flow. In figure 5(*b*), we plot the first, second, third and fifth tank-treading periods. The period shows a linear variation with the elastic capillary number. It shows a higher value for the first tank-treading period when the capsule is closest to the wall. As the capsule moves laterally away from the wall, the tank-treading period decreases. The underlying physics can be understood from figure 5(*a*). Near the wall, a capsule experiences higher deformation caused by the excess stress due to the wall effect. The tank-treading period is the time for the fluid particle to complete the motion around the capsule. The more deformed the interface, the longer it takes for the fluid particle to go around. As the deformed capsule moves away from the wall, the deformation decreases, resulting in a lower tank-treading period. For a capsule in an unbounded

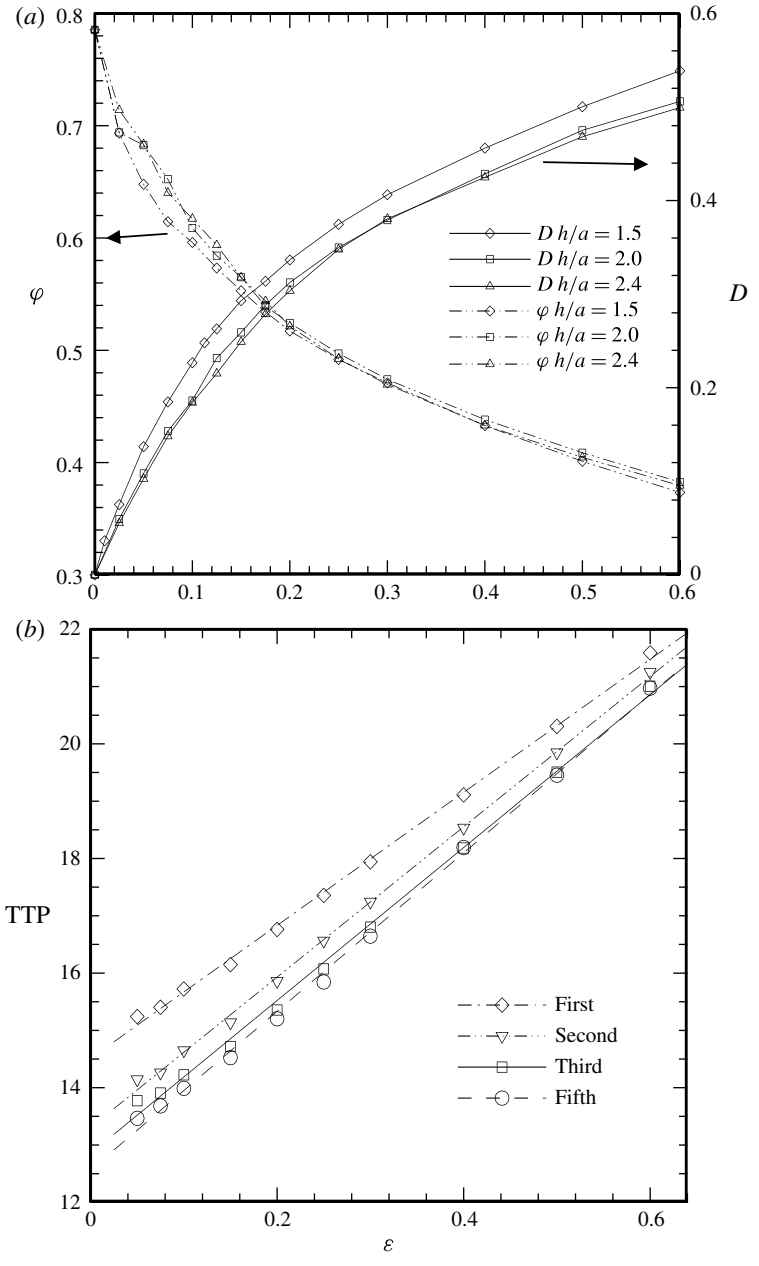

FIGURE 5. (*a*) Deformation D and orientation angle φ, and (*b*) first, second, third and fifth tank-treading periods (TTP) versus capillary number (ε) for an NH capsule at $\lambda = 1$.

shear, we saw a one-to-one relation between the deformation and the tank-treading period (Lac *et al.* 2004; Li & Sarkar 2008). Further, closeness to the wall retards the membrane motion.

The migration of a drop in a shear flow near a wall has been extensively investigated (Uijttewaal *et al.* 1993). Due to the similarity between the capsule and drop cases, in figure 6, we compare the migration of a drop and an NH capsule as

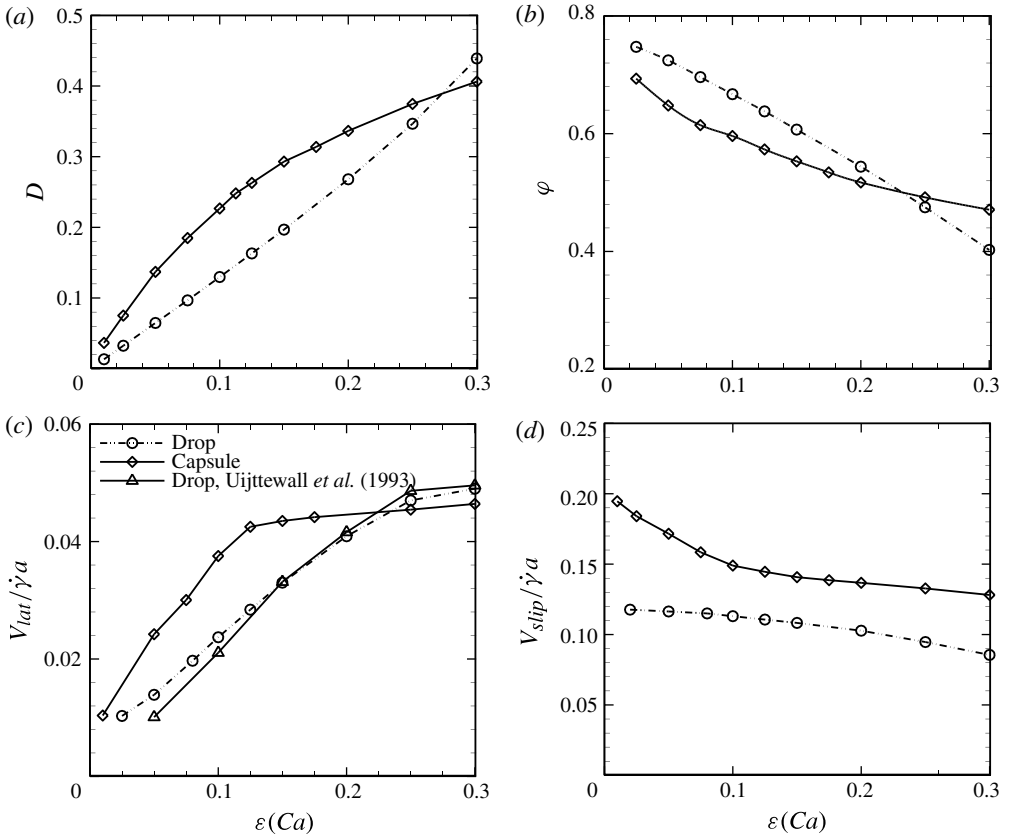

FIGURE 6. Comparison of (*a*) deformation, (*b*) orientation angle, (*c*) lateral velocity and (*d*) slip velocity versus capillary number for an NH capsule and a viscous drop at $h/a = 1.5$.

a function of capillary number $\varepsilon = \mu\dot{\gamma}a/G_s$ and $Ca = \mu\dot{\gamma}a/\sigma_s$ at a fixed separation $h/a = 1.5$. In figure 6(*a,b*), we observe that the variations of deformation and orientation angle for a drop and a capsule show distinct characteristics with capillary numbers. For low capillary numbers, deformation of both capsules and drops increases linearly with capillary number $\varepsilon(Ca)$. At low capillary numbers below $\varepsilon(Ca) \simeq 0.25$, a capsule reaches a larger deformation and smaller orientation angle compared to a drop. The opposite occurs at higher capillary numbers above $\varepsilon(Ca) > 0.28$. The inclination angle variation with capillary number shows similar crossover between a drop and a capsule, the capsule initially decreasing its inclination with $\varepsilon(Ca)$ faster than the drop and later reversing.

The migration velocity shows roughly linear variation with $\varepsilon(Ca)$ for smaller values of these numbers (figure 6*c*). The linearity is replaced by a quadratic variation for drops at larger Ca, but for capsules the migration velocity seems to be flatter ($\sim\varepsilon^{0.6}$: see (4.18)) for $\varepsilon > 0.1$. The drop migration velocity compares very well with the boundary element method (BEM) computation of Uijttewaal *et al.* (1993), also shown here. For larger capillary numbers ($Ca > 0.3$), the migration velocity of a drop experiences different dynamics initially, and only at a larger wall separation does it reach a quasi-steady state. Figure 6(*d*) shows that the slip velocity of a migrating drop is at least initially independent of capillary number (note that the perturbative

theory – (4.7) below – due to Shapira & Haber 1990 obtains a value 0.0972 for the slip velocity of a drop at $h/a = 1.5$ close enough to the simulated value of 0.11). However, for a capsule, the slip velocity shows an initial linear decrease followed by a region of little change. In the next section, we try to explore some of these variations using relations analogous to those for drops obtained using perturbative analysis.

4.3. *Quasi-steady dynamics: scaling with distance and elastic capillary number*

For a viscous drop with a Newtonian interface characterized by an interfacial tension value, perturbative theories predict a number of scaling relations. Due to the similarity between a drop and a capsule, we are led to investigate similar scalings for capsules. Shapira & Haber (1990) arrived at an expression for deformation of a drop induced by the presence of the wall:

$$D = D_{Taylor}\left[1 + \frac{3(1+2.5\lambda)}{8(1+\lambda)}\left(\frac{a}{h}\right)^3\right], \quad D_{Taylor} = \frac{(16+19\lambda)}{16(1+\lambda)}Ca, \tag{4.5}$$

where D_{Taylor} is the deformation of a drop in free shear obtained using a perturbative method by Taylor (1934). The expression was also successfully matched by BEM simulation at low capillary numbers (Uijttewaal *et al.* 1993). Figure 7(*a*) shows that the deformation of a capsule also scales as $D \sim (a/h)^3$ for different ε values. Figure 6(*a*) already showed linear variation of D with ε for small ε. For the lateral migration of a viscous drop, Chan & Leal (1979) obtained an analytical expression:

$$\frac{V_{lat}}{\dot{\gamma}a} = D_{Taylor}\frac{3\left(54\lambda^2+97\lambda+54\right)}{280(1+\lambda)^2}\left(\frac{a}{h}\right)^2. \tag{4.6}$$

Figure 7(*b*) shows that for capsules too, $V_{lat} \sim (a/h)^2$ for low ε (see § 4.5). In figure 7(*c*), we show a scaling similar to (4.6) $V_{lat} \sim D(a/h)^2$. Note that Chan & Leal, in their perturbative analysis, did not account for effects of the wall on drop deformation, and took it to be D_{Taylor}. Instead, here we use the simulated instantaneous deformation D at that position. The scaling is again better for lower values of $D(a/h)^2$ corresponding to a larger capsule–wall distance (h). In the inset of figure 7(*c*), we also show the analogous scaling (4.6) for a viscous drop: the scaling is far better for the drop than for the capsule. For the slip velocity of a viscous drop, Shapira & Haber (1990) obtained

$$\frac{V_{slip}}{\dot{\gamma}a} = \left(\frac{a}{h}\right)^2\frac{1+2.5\lambda}{8(1+\lambda)}. \tag{4.7}$$

In figure 7(*d*), we see that for a capsule, the slip velocity follows a similar scaling $V_{slip} \sim (a/h)^2$ scaling being better for lower ϵ.

Note that there have been extensive studies of vesicle and RBC migration in wall-bounded shear flows predicting and numerically verifying inverse square variation with wall separation (Olla 1997*a*,*b*, 1999; Sukumaran & Seifert 2001; Farutin & Misbah 2013). Typically, the vesicles have a volume less than the maximal volume for their area. Olla (1997*a*) obtained a relation $V_{lat} = U(\lambda, B/L, W/L)\dot{\gamma}LBW/h^2$ for an ellipsoidal vesicle with principal axes L, B and W, where $U(\lambda, B/L, W/L)$ is a function of the parameters indicated. The inverse square law was also experimentally observed (Callens *et al.* 2008; Grandchamp *et al.* 2013). Sukumaran & Seifert (2001) using a BEM simulation found a correlation $V_{lat} = 0.08\dot{\gamma}LBW/h^2$ for a vesicle of close to maximal (95 %) volume.

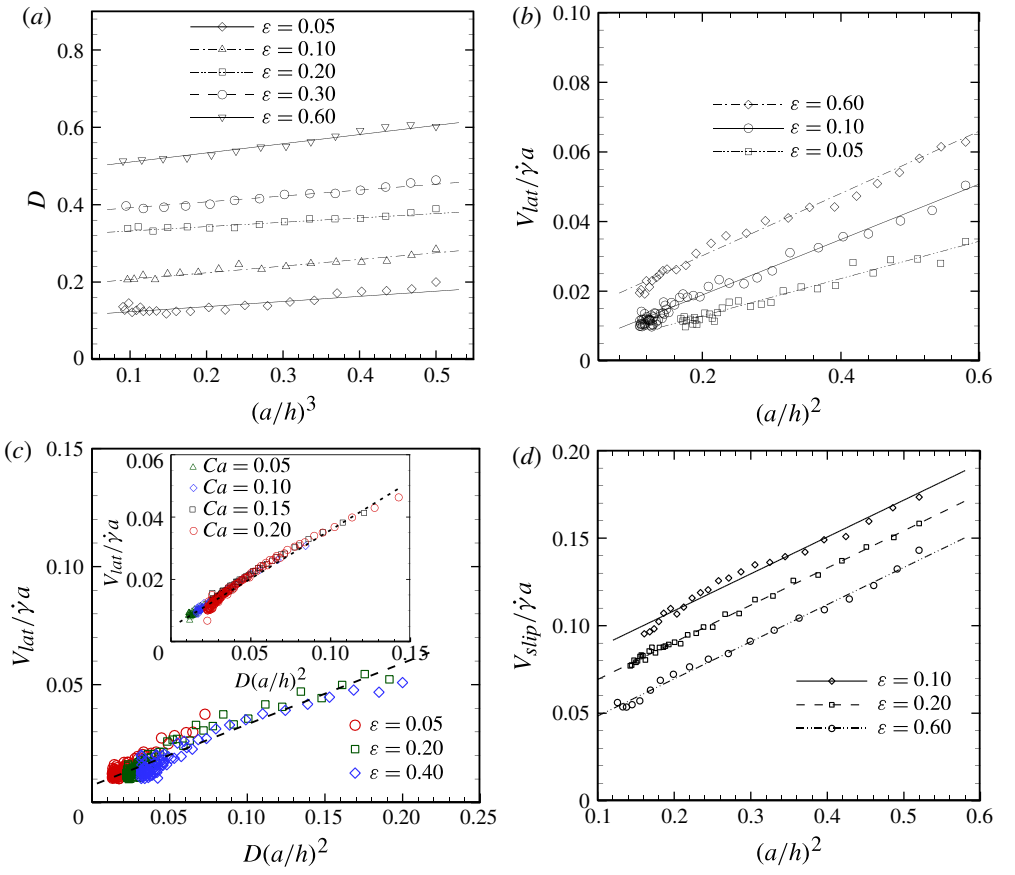

FIGURE 7. (Colour online) Scalings of different parameters with capsule–wall distances (h/a): (a) deformation versus $(a/h)^3$, (b) lateral velocity versus $(a/h)^2$, (c) lateral velocity versus $D(a/h)^2$ (the inset shows the same for a viscous drop) and (d) slip velocity versus $(a/h)^2$.

4.4. *A far-field theory of lateral migration velocity*

In the previous section, we used analytical theories for migration of a viscous drop to postulate analogous expressions for a capsule. We did not find any perturbative analysis in the literature for the lateral migration of a capsule in shear flow. Although one can do such an analysis, investigating any of the previous studies for drops amply demonstrates the algebraic complexity of the task. Furthermore, although it provides an analytical expression, the underlying physics remains non-transparent. As mentioned in the Introduction, Smart & Leighton (1991) elucidated the migration of a viscous drop near a wall as arising from the image stresslet field induced by the presence of a wall. Here, we develop this idea to explain the scaling that we presented in the last section. Note that the derivation here closely follows a recent investigation for drop migration in a viscoelastic medium by us (Mukherjee & Sarkar 2013). Therefore we provide a brief sketch for completeness and omit details. We express the flow field using a Stokes Green's function, as is usually done in boundary element simulations. Assuming Stokes flow, the velocity field outside the capsule in

the entire domain can be written as

$$\left.\begin{aligned} u_j(\boldsymbol{x}) &= u_j^{\infty} - \frac{1}{8\pi\mu_m}\int_{A_d} f_i(\boldsymbol{y})G_{ij}(\boldsymbol{x},\boldsymbol{y})\,\mathrm{d}A(\boldsymbol{y}) \\ &\quad + \frac{(1-\lambda)}{8\pi}\int_{A_d} u_i(\boldsymbol{y})M_{ijk}(\boldsymbol{x},\boldsymbol{y})n_k(\boldsymbol{y})\,\mathrm{d}A(\boldsymbol{y}), \\ G_{ij}(\boldsymbol{x},\boldsymbol{y}) &= G_{ij}^{FS}(\boldsymbol{x},\boldsymbol{y}) + G_{ij}^{w}(\boldsymbol{x},\boldsymbol{y}), \quad M_{ijk}(\boldsymbol{x},\boldsymbol{y}) = M_{ijk}^{FS}(\boldsymbol{x},\boldsymbol{y}) + M_{ijk}^{w}(\boldsymbol{x},\boldsymbol{y}), \end{aligned}\right\} \tag{4.8}$$

where we use the proper Green's function that adds a contribution $G_{ij}^{w}(\boldsymbol{x},\boldsymbol{y})$ to the free space Green's function $G_{ij}^{FS}(\boldsymbol{x},\boldsymbol{y})$ so that $G_{ij}(\boldsymbol{x},\boldsymbol{y}) = 0$ on the wall $y_2 = 0$ (Blake 1971). The tensor $M_{ijk}(\boldsymbol{x},\boldsymbol{y})$ is the stress due to this Green's function. This special property of the Green's function along with the no-slip condition eliminates the surface integral over the wall. Here u_i^{∞} is the imposed shear, A_d is the surface of the capsule with outward normal $n_i(\boldsymbol{x})$, and $f_i(\boldsymbol{x})$ is the membrane force appearing in (2.1) which is also equal to the jump in fluid traction across the membrane (see (4.13) below). We find an expression appropriate for the far-field by performing a Taylor series expansion of the Green's function and the double-layer potential around the centre of the drop $\boldsymbol{y}_c$:

$$G_{ij}(\boldsymbol{x},\boldsymbol{y}) = G_{ij}(\boldsymbol{x},\boldsymbol{y}_c) + \frac{\partial G_{ij}(\boldsymbol{x},\boldsymbol{y}_c)}{\partial y_{ck}}(y_k - y_{ck}) + O\left(\frac{a}{|\boldsymbol{y}-\boldsymbol{y}_c|}\right)^3, \tag{4.9}$$

$$M_{ijk}(\boldsymbol{x},\boldsymbol{y}) = M_{ijk}(\boldsymbol{x},\boldsymbol{y}_c) + O\left(\frac{a}{|\boldsymbol{y}-\boldsymbol{y}_c|}\right)^3. \tag{4.10}$$

Using this expression in (4.8), and noting that $\int_{A_d} f_j(\boldsymbol{y})\,\mathrm{d}A(\boldsymbol{y}) = 0$ (net membrane force for a free capsule) and $\int_{A_d} u_k(\boldsymbol{y})n_k(\boldsymbol{y})dA(\boldsymbol{y}) = 0$ (incompressibility), we obtain the far-field expression of the velocity field given in terms of the stresslet

$$\begin{aligned} u_j(\boldsymbol{x}) &= u_j^{\infty}(\boldsymbol{x}) - \frac{1}{8\pi\mu_m}\frac{\partial G_{ij}(\boldsymbol{x},\boldsymbol{y}_c)}{\partial y_{ck}} \\ &\quad \times \left\{\int_{A_d} f_i(\boldsymbol{y})(y_k - y_{ck})\,\mathrm{d}A(\boldsymbol{y}) - \mu_m(1-\lambda_\mu)\int_{A_d}(u_i n_k + u_k n_i)(\boldsymbol{y})\,\mathrm{d}A(\boldsymbol{y})\right\} \\ &= u_j^{\infty}(\boldsymbol{x}) - \frac{1}{8\pi\mu_m}\frac{\partial G_{ij}(\boldsymbol{x},\boldsymbol{y}_c)}{\partial y_{ck}}(S_{ik}^{mem\prime} + S_{ik}^{vrat\prime}) \\ &= u_j^{\infty}(\boldsymbol{x}) - \frac{1}{8\pi\mu_m}\frac{\partial G_{ij}(\boldsymbol{x},\boldsymbol{y}_c)}{\partial y_{ck}}(S_{ik}^{mem} + S_{ik}^{vrat}), \end{aligned} \tag{4.11}$$

where

$$S_{ik}^{mem\prime} = \int_{A_d} f_i(\boldsymbol{y})(y_k - y_{ck})\,\mathrm{d}A(\boldsymbol{y}), \tag{4.12a}$$

$$S_{ik}^{vrat\prime} = -\mu_m(1-\lambda_\mu)\int_{A_d}(u_i n_k + u_k n_i)(\boldsymbol{y})\,\mathrm{d}A(\boldsymbol{y}) \tag{4.12b}$$

are the contributions to the stresslet due to the interfacial stresses and the viscosity ratio respectively. The same terms without primes in the last expression in (4.11) represent their traceless forms. Note that due to incompressibility, $\partial G_{ik}(\boldsymbol{x},\boldsymbol{y}_c)/\partial y_{ck} = 0$. Therefore, the traces of the stresslets do not contribute. Also, note that the theory is identical for a drop and a capsule, the only difference being that the interfacial or membrane stress terms are different in the two cases (Mukherjee & Sarkar 2013). For

a drop, the relation

$$f_i(\boldsymbol{y}) = \sigma_s n_i(\boldsymbol{y})[\nabla \cdot \boldsymbol{n}(y)] \tag{4.13}$$

gives rise to

$$S_{ik}^{mem\prime} = \sigma_s \int_{A_d} (\delta_{ik} - n_i n_k)\, \mathrm{d}A(\boldsymbol{y}), \tag{4.14}$$

where an identity due to Rosenkilde (1967) has been used to change the surface integral term involving curvature (4.12) and (4.13).

The drop or capsule migration is caused by the velocity field due to the image stresslet induced by the wall, i.e. the contribution due to $G_{ij}^{w}(\boldsymbol{x}, \boldsymbol{y})$ in (4.8) towards $\partial G_{ij}(\boldsymbol{x}, \boldsymbol{y}_c)/\partial y_{ck}$ in (4.11). Smart and Leighton obtained an expression for the image stresslet propagator near a rigid wall with normal $\boldsymbol{n}$. Using that, one obtains the lateral velocity as

$$u_j^{drift} n_j = -\frac{1}{8\pi\mu_m}\left(\frac{9}{8h^2}\right)(S_{ik}^{mem} + S_{ik}^{vrat}) n_i n_k, \quad \left(\frac{a}{h}\right)^2 \ll 1. \tag{4.15}$$

For the case here with the wall at $x_2 = 0$, we obtain the migration velocity

$$V_{lat} = -\frac{1}{8\pi\mu_m}\left(\frac{9}{8h^2}\right)(S_{22}^{mem} + S_{22}^{vrat}). \tag{4.16}$$

Non-dimensionalizing, we obtain

$$\frac{V_{lat}}{\dot{\gamma} a} = -\frac{9}{64\pi}\left(\frac{a}{h}\right)^2 (S_{22}^{mem*} + S_{22}^{vrat*}) = -0.4476\left(\frac{a}{h}\right)^2 (S_{22}^{mem*} + S_{22}^{vrat*}), \tag{4.17}$$

where non-dimensional stresslet $S_{22}^{*} = S_{22}/\dot{\gamma}\mu_m a^3$. The second term is absent for a viscosity matched system ($\lambda_\mu = 1$). In figure 8(*a*), we plot the simulated migration velocity as a function of the distance from the wall and compare it with the expression obtained by the stresslet theory (4.17) for different ε. The two curves match well for large separation from the wall, $h/a \geqslant 2.5$, where the one-term series expansion (4.9) is valid, but not for small h/a. However, note also that the higher-order terms in (4.9) would lead to a correction of order $(h/a)^3$. On the other hand, the relationship $V_{lat}/\dot{\gamma} a \sim (a/h)^2$ is seen to hold even for smaller h/a, at least for the small ε considered here (see § 4.5 for deviation from this scaling at larger ε). At any rate, to investigate this theory further, we plot in figure 8(*b*) the migration velocity against $S_{22}^{*}(a/h)^2$ for different wall separation h and elastic capillary number ε. They collapse to a single curve as predicted by (4.17). In figure 8(*c*), we show that the stresslet theory works better for a viscous drop. In figure 8(*d*), we investigate the dependence of S_{22}^{mem} on capillary number for drops and elastic capillary number for capsules. Both show linear variation for small values of the capillary numbers. This is consistent with (4.6) in view of the relation $D \sim Ca$ as well as the results plotted in figure 7(*c*). As noted before, the linearity breaks down for capsules before it happens for drops.

4.5. *A phenomenological correlation for migration velocity*

The above result implies a power law relation for the capsule migration velocity. Using the simulated results, we seek such a phenomenological relation as a function of ε and h/a. However, although we find $V_{lat}/\dot{\gamma} a \sim \varepsilon(a/h)^2$ for small ε, in figures 6(*c*) and 8(*d*) one clearly sees a deviation from linearity for larger ε. For larger ε, we also find deviation from $V_{lat}/\dot{\gamma} a \sim (a/h)^2$: the inset of figure 9(*a*) shows that $V_{lat}(h/a)^2/\dot{\gamma} a$ as a

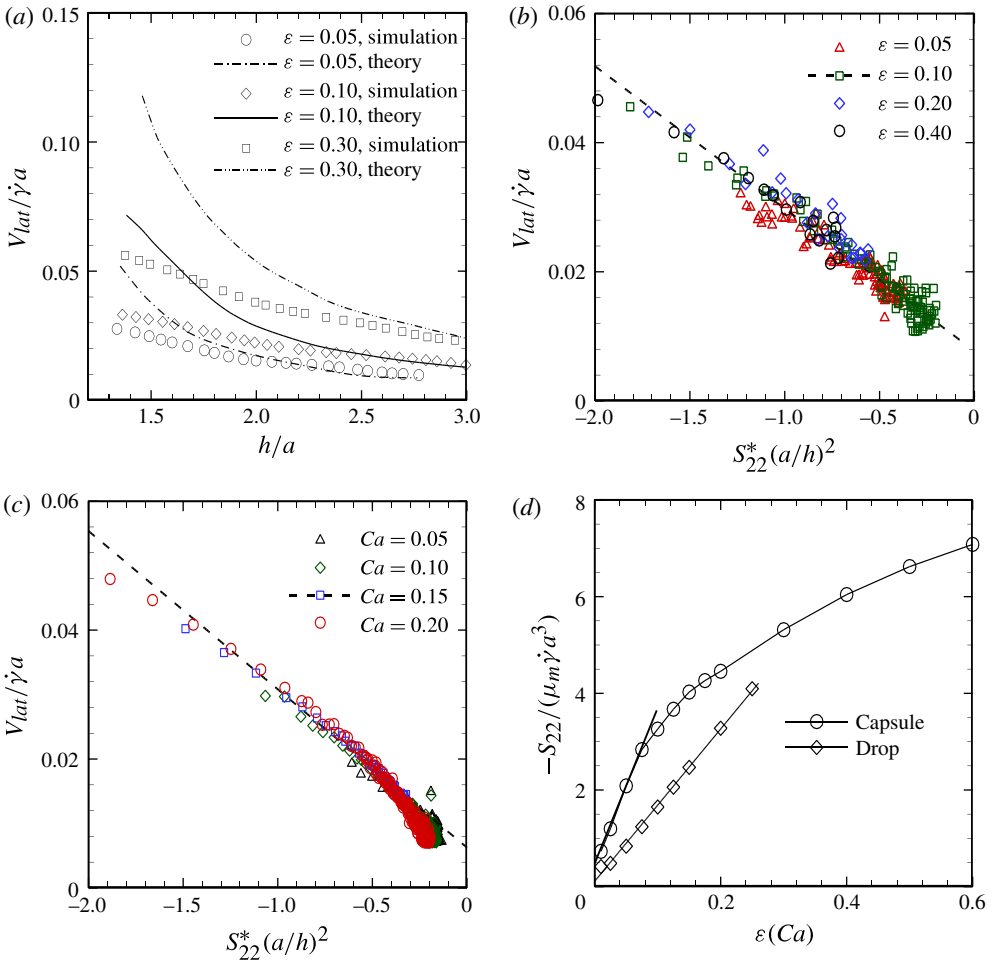

FIGURE 8. (Colour online) (*a*) Comparison of lateral velocity between simulation and theory (21) for different ε values. Variation of lateral velocity with stresslet for a capsule (*b*) and a drop (*c*) at different capillary numbers. Away from the wall, all curves converge to single one for both cases. (*d*) Comparison of the variation of S_{22} with capillary number for a drop and a capsule at $h = 1.5a$.

function of ε for different h/a fails to collapse to a single curve, especially for larger ε. The main plot in figure 9(*a*) shows that, in fact, in this range $V_{lat}/\dot{\gamma}a \sim (a/h)^{1.35}$. Using the simulated result, we propose the following relation:

$$\left.\begin{aligned} &\frac{V_{lat}}{\dot{\gamma}a} = (0.65\varepsilon + 0.021)\left(\frac{a}{h}\right)^2 \quad \varepsilon \leqslant \varepsilon_{cr}, \\ &\frac{V_{lat}}{\dot{\gamma}a} = \frac{V_{lat}}{\dot{\gamma}a}\bigg|_{\varepsilon=\varepsilon_{cr}} + 0.02(\varepsilon - \varepsilon_{cr})^{0.6}\left(\frac{a}{h}\right)^{1.35} \quad \varepsilon > \varepsilon_{cr}, \\ &0.125 < \varepsilon_{cr} < 0.175. \end{aligned}\right\} \tag{4.18}$$

The finite intercept at $\varepsilon = 0$ might be attributed to the finite inertia present in the simulation. Here ε_{cr} is the value of elastic capillary number where the linearity with ε breaks down and $\varepsilon^{0.6}$ is observed. Note that 0.6 power scaling with the capillary was also recently found by Pranay *et al.* (2012). The simulation suggests that for $\varepsilon > \varepsilon_{cr}$

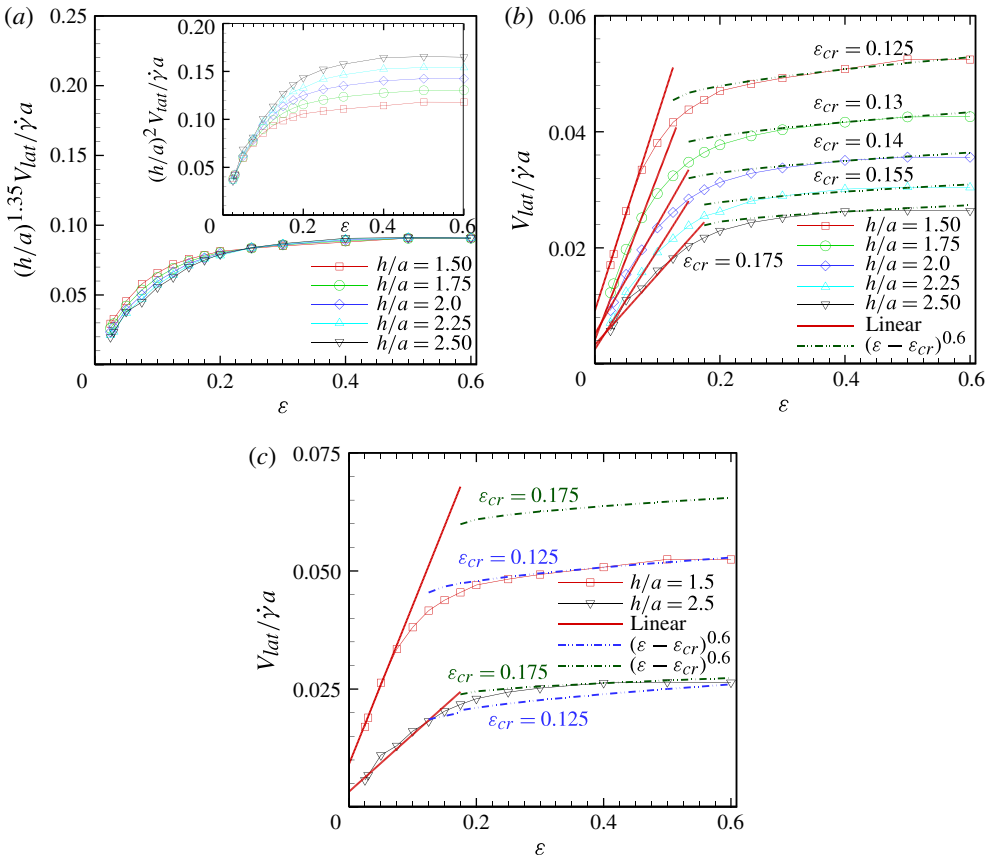

FIGURE 9. (Colour online) (*a*) $V_{lat}(h/a)^{1.35}/\dot{\gamma}a$ versus ε. The inset shows variation of $V_{lat}(h/a)^2\dot{\gamma}a$ with ε. (*b*) Empirical expression (4.18) plotted along with simulated results. (*c*) Comparison of migration velocity from expression (4.18) using upper and lower limits of ε_{cr} with simulation at two wall separations.

the quadratic scaling with inverse distance from the wall also ceases to hold. However, ε_{cr} seems to vary with h/a within a small range $0.125 < \varepsilon_{cr} < 0.175$, being larger for larger h/a. Figure 9(*b*) shows that choosing appropriate ε_{cr} for different h/a provides a good match between the correlation (4.18) and the simulated velocity. However, one would like to obtain an *a priori* estimate of ε_{cr} for (4.18) to be useful. Using the maximum and the minimum values of ε_{cr} for the smallest and the largest h/a considered here, figure 9(*c*) shows that the two limits provide an upper and a lower bound for the migration velocity. As can be expected, the result is more sensitive closer to the wall $h/a = 1.5$, where the appropriate value is the lower limit $\varepsilon_{cr} \sim 0.125$. Using this value leads to less than 20 % error, even for the largest h/a considered here (figure 9*c*). In the next subsection, we investigate the effects of the viscosity ratio on the correlation (4.18).

4.6. *Effects of the viscosity ratio and membrane constitutive law*

In figure 10 we consider the effects of the viscosity ratio. Figure 10(*a*) shows the quasi-steady capsule migration velocity as a function of viscosity ratio for $h/a = 1.5$

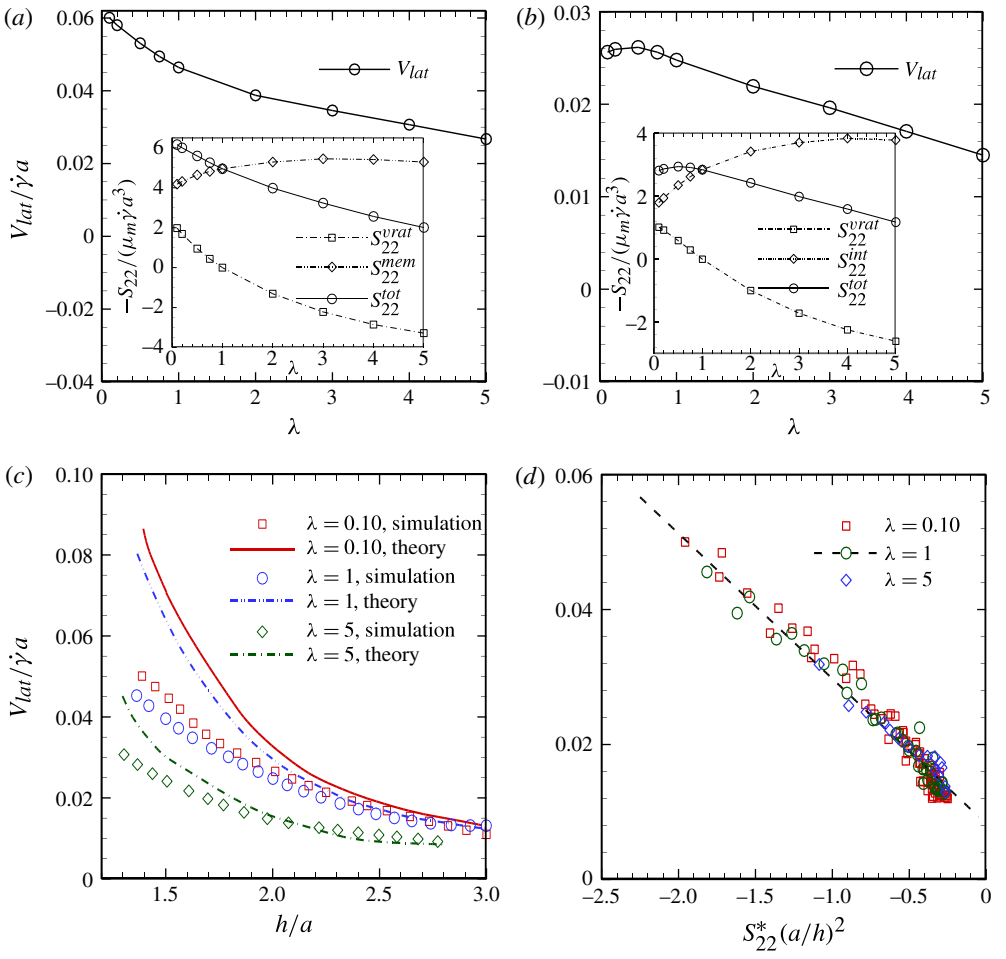

FIGURE 10. (Colour online) Variation of (*a*) lateral velocity of a capsule with λ at $h/a = 1.5$ and $\varepsilon = 0.30$. The inset shows the variations of $-S_{22}^{tot}$, $-S_{22}^{vrat}$ and $-S_{22}^{mem}$ with λ for the same case. (*b*) Variation of lateral velocity of a drop with λ at $h/a = 1.5$ and $Ca = 0.20$. The inset shows the variation of $-S_{22}^{tot}$, $-S_{22}^{vrat}$ and $-S_{22}^{int}$ with λ for the same case. (*c*) Comparison of simulated lateral velocity and that from the stresslet theory at three λ values at $\varepsilon = 0.10$. (*d*) Variation of lateral velocity with $S_{22}^{*}(a/h)^2$ for a capsule at $\varepsilon = 0.10$. Away from the wall, all curves converge to a single one.

and $\varepsilon = 0.3$. The migration velocity decreases with increasing viscosity ratio. Note that as the viscosity inside the capsule increases, the capsule behaviour approaches that of a rigid particle, which does not experience any lateral motion in a Stokes flow. We also investigate the stresslet theory (4.17) developed in § 4.4. In the inset, we plot the total stresslet S_{22}^{tot} along with the contributions S_{22}^{mem} and S_{22}^{vrat} due to the membrane and the viscosity ratio terms. Note that the membrane term S_{22}^{mem} increases as the viscosity ratio increases from $\lambda = 1$. The result is, however, dominated by S_{22}^{vrat}, which drastically reduces with λ. Figure 10(*b*) shows the same physics for a drop at $Ca = 0.2$ and $h/a = 1.5$. Figure 10(*c*) shows a direct comparison of the stresslet theory and the simulated capsule migration velocity as a function of h/a for different λ. Similar to the viscosity matched case, here also the theory works well at large separation from

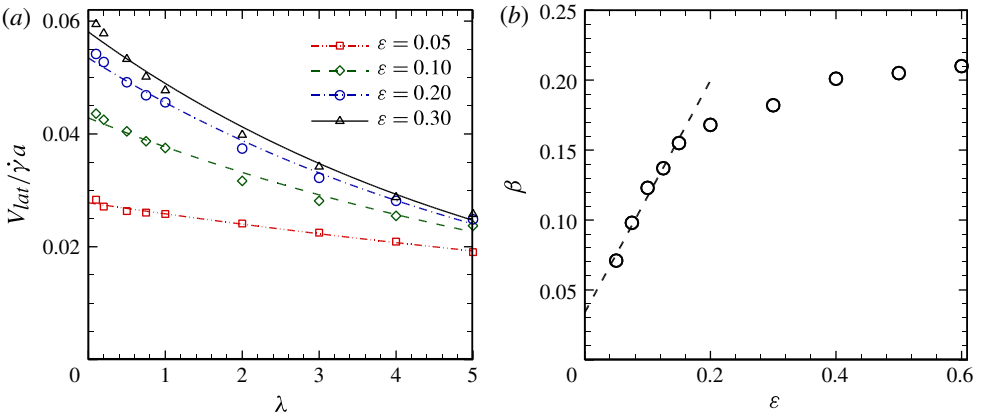

FIGURE 11. (Colour online) (*a*) Variation of the lateral velocity with viscosity ratio. (*b*) Variation of β with capillary numbers.

wall $h/a \geqslant 2.5$. In figure 10(*d*), we show that the migration velocity plotted as a function of $S_{22}^{*}(a/h)^2$ according to (4.17) collapses to a single curve for three different viscosity ratios.

In § 4.5, we developed a phenomenological correlation of capsule migration velocity as a function of ε and a/h. Figure 11(*a*) shows that the migration velocity decreases exponentially with viscosity ratio, giving rise to a correlation

$$\frac{V_{lat}}{\dot{\gamma}a} = \frac{V_{lat}}{\dot{\gamma}a}\bigg|_{\lambda=1} \mathrm{e}^{-\beta(\varepsilon)(\lambda-1)}. \tag{4.19}$$

Note that due to the exponential variation, in the limit of infinite viscosity ratio, one recovers zero migration for a rigid sphere. The exponential power β increases linearly with ε for small ε and later seems to approach $\beta \sim 0.2$ (figure 11*b*). The expression at $\lambda = 1 V_{lat}/\dot{\gamma}a|_{\lambda=1}$ is given by (4.18).

Finally, we very briefly study the effects of the membrane constitutive law – NH, SK ($C = 1$), SK ($C = 10$) and ES ($A = 3$) – on the migration of a capsule for $\lambda = 1$ in figure 12. Note that the neo-Hookean model is strain softening and is easier to deform than that of the Skalak membrane, which is a strain hardening model (Barthes-Biesel *et al.* 2002). The migration velocity plotted as a function of ε at $h/a = 1.5$, however, shows very similar results for all constitutive laws. For NH, SK ($C = 1$) and ES ($A = 3$), the migration velocity is indistinguishable. SK ($C = 10$) leads to a decreased migration velocity. The behaviour for slip velocity is also similar except that SK ($C = 10$) leads to higher slip velocity.

5. Summary

We have investigated the migration dynamics of a capsule enclosed by an elastic membrane in shear near a wall using a front-tracking method, and compared its dynamics with that of a drop. A spherical capsule initially deforms quickly and reaches a quasi-steady state just like a viscous drop, where the dynamics – deformation, migration and slip velocities – depend only on the instantaneous capsule–wall distance, independent of its initial history. Both migration and slip velocities of the capsule vary approximately as the square of the inverse of the

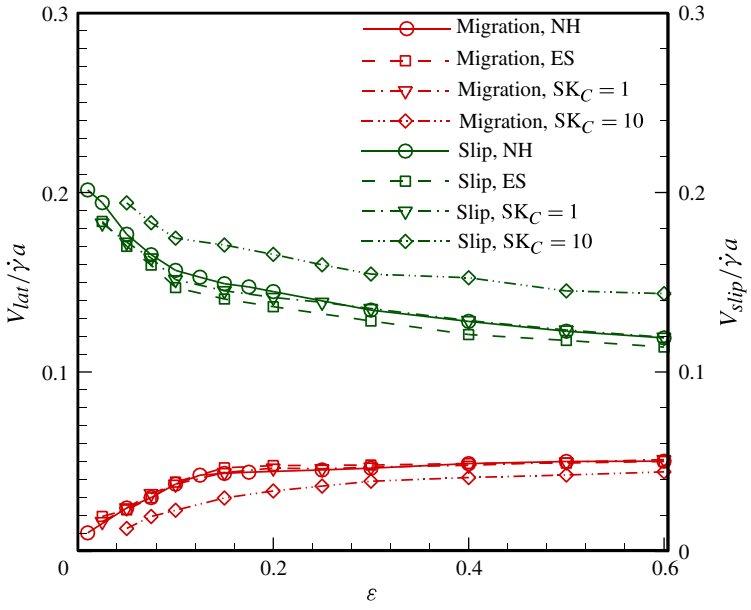

FIGURE 12. (Colour online) Variation of migration and slip velocities with ε for different membrane constitutive laws at $h/a = 1.5$ and $\lambda = 1$.

distance from the wall whereas the deformation varies with the inverse cube of the distance. These scalings are very similar to those predicted by the perturbative theories for drops.

We developed a semi-analytic theory of migration velocity by representing the flow field using a Green's function that automatically accounts for the presence of the wall. The theory clearly shows that the presence of the capsule gives rise to a stresslet in the far field, and the migration is a result of the velocity field induced by the image stresslet on the other side of the wall. The theory predicts the inverse square variation with the wall separation, quantitatively matching the simulated velocity away from the wall $h/a \geqslant 2.5$. Furthermore, it delineates the two distinct additive contributions to the stresslet due to the viscosity ratio and the membrane stresses. With increasing viscosity ratio, although the membrane stresslet term increases, the migration velocity decreases due to the larger decrease in the stresslet term directly related to the viscosity ratio.

Inspired by the different scalings seen in the simulation and the small deformation perturbative results for drops, we proposed a correlation for capsule migration as a function of capillary number, wall distance and viscosity ratio. It shows two distinct regimes – smaller than a critical capillary number ε_{cr}, $V_{lat}/\dot{\gamma}a \sim \varepsilon(a/h)^2$ and above, $V_{lat}/\dot{\gamma}a \sim (\varepsilon - \varepsilon_{cr})^{0.6}(a/h)^{1.35}$. With viscosity ratio λ, $V_{lat}/\dot{\gamma}a \sim \mathrm{e}^{-\beta(\lambda-1)}$. Different constitutive equations for the membrane elasticity seem to produce similar migration.

Acknowledgements

K.S. acknowledges valuable discussions with Professor M. Graham of the University of Wisconsin, which was critical for understanding an error in our earlier interpretation of the simulated results and a subsequent change of course leading to the development of the image stresslet theory. K.S. acknowledges partial financial

support from the University of Delaware Research Foundation, NSF grants CBET-0625599, CBET-0651912, CBET-1033256, DMR-1239105, CBET-1205322 and NIH grant P20RR016472.

REFERENCES

ABKARIAN, M. & VIALLAT, A. 2005 Dynamics of vesicles in a wall-bounded shear flow. *Biophys. J.* **89**, 1055–1066.

AGGARWAL, N. & SARKAR, K. 2007 Deformation and breakup of a viscoelastic drop in a Newtonian matrix under steady shear. *J. Fluid Mech.* **584**, 1–21.

AGGARWAL, N. & SARKAR, K. 2008*a* Effects of matrix viscoelasticity on viscous and viscoelastic drop deformation in a shear flow. *J. Fluid Mech.* **601**, 63–84.

AGGARWAL, N. & SARKAR, K. 2008*b* Rheology of an emulsion of viscoelastic drops in steady shear. *J. Non-Newtonian Fluid Mech.* **150**, 19–31.

BAGCHI, P. & KALLURI, R. M. 2009 Dynamics of nonspherical capsules in shear flow. *Phys. Rev.* E (80)016307.

BARBEE, J. H. & COKELET, G. R. 1971 Fahraeus effect. *Microvasc. Res.* **3**, 6–16.

BARTHES-BIESEL, D. 1980 Motion of a spherical microcapsule freely suspended in a linear shear flow. *J. Fluid Mech.* **100**, 831–853.

BARTHES-BIESEL, D., DIAZ, A. & DHENIN, E. 2002 Effect of constitutive laws for two-dimensional membranes on flow-induced capsule deformation. *J. Fluid Mech.* **460**, 211–222.

BARTHES-BIESEL, D. & RALLISON, J. M. 1981 The time-dependent deformation of a capsule freely suspended in a linear shear flow. *J. Fluid Mech.* **113**, 251–267.

BLAKE, J. R. 1971 Image system for a Stokeslet in a no-slip boundary. *Proc. Camb. Phil. Soc.* **70**, 303–310.

CALLENS, N., MINETTI, C., COUPIER, G., MADER, M. A., DUBOIS, F., MISBAH, C. & PODGORSKI, T. 2008 Hydrodynamic lift of vesicles under shear flow in microgravity. *Eur. Phys. Lett.* (83)24002.

CANTAT, I. & MISBAH, C. 1999 Lift force and dynamical unbinding of adhering vesicles under shear flow. *Phys. Rev. Lett.* **83**, 880–883.

CHAFFEY, C. E., BRENNER, H. & MASON, S. G. 1965 Particle motions in sheared suspensions. XVIII. Wall migration (theoretical). *Rheol. Acta* **4**, 64–72.

CHAN, P. C. H. & LEAL, L. G. 1979 Motion of a deformable drop in a second-order fluid. *J. Fluid Mech.* **92**, 131–170.

COUPIER, G., KAOUI, B., PODGORSKI, T. & MISBAH, C. 2008 Noninertial lateral migration of vesicles in bounded Poiseuille flow. *Phys. Fluids* (20)111702.

DAMIANO, E. R., WESTHEIDER, J., TOZEREN, A. & LEY, K. 1996 Variation in the velocity, deformation, and adhesion energy density of leukocytes rolling within venules. *Circulat. Res.* **79**, 1122–1130.

DODDI, S. K. & BAGCHI, P. 2008 Lateral migration of a capsule in a plane Poiseuille flow in a channel. *Intl J. Multiphase Flow* **34**, 966–986.

DODDI, S. K. & BAGCHI, P. 2009 Three-dimensional computational modelling of multiple deformable cells flowing in microvessels. *Phys. Rev.* E (79)046318.

EGGLETON, C. D. & POPEL, A. S. 1998 Large deformation of red blood cell ghosts in a simple shear flow. *Phys. Fluids* **10**, 1834–1845.

EVANS, E. A. & SKALAK, R. 1979 Mechanics and thermodynamics of biomembranes. Part 2. *CRC Critical Rev. Bioengng* **3**, 331–418.

FÅHRAEUS, R. 1929 The suspension stability of blood. *Phys. Rev.* **9**, 241–274.

FARUTIN, A. & MISBAH, C. 2013 Analytical and numerical study of three main migration laws for vesicles under flow. *Phys. Rev. Lett.* (110)108104.

GRANDCHAMP, X., COUPIER, G., SRIVASTAV, A., MINETTI, C. & PODGORSKI, T. 2013 Lift and down-gradient shear-induced diffusion in red blood cell suspensions. *Phys. Rev. Lett.* (110)108101.

IMAEDA, T. 2000 Shear-induced migration of a droplet in the presence of a plane wall. *Physica* A **285**, 306–314.

KAOUI, B., RISTOW, G. H., CANTAT, I., MISBAH, C. & ZIMMERMANN, W. 2008 Lateral migration of a two-dimensional vesicle in unbounded Poiseuille flow. *Phys. Rev.* E **77**, 021903.

KARNIS, A. & MASON, S. G. 1967 Particle motions in sheared suspensions. XXIII. Wall migration of fluid drops. *J. Colloid Interface Sci.* **24**, 164–169.

KENNEDY, M. R., POZRIKIDIS, C. & SKALAK, R. 1994 Motion and deformation of liquid drops, and the rheology of dilute emulsions in simple shear flow. *Comput. Fluids* **23**, 251–278.

LAC, E., BARTHES-BIESEL, D., PELEKASIS, N. A. & TSAMOPOULOS, J. 2004 Spherical capsules in three-dimensional unbounded Stokes flows: effect of the membrane constitutive law and onset of buckling. *J. Fluid Mech.* **516**, 303–334.

LEAL, L. G. 1980 Particle motions in a viscous fluid. *Annu. Rev. Fluid Mech.* **12**, 435–476.

LEFEBVRE, Y. & BARTHES-BIESEL, D. 2007 Motion of a capsule in a cylindrical tube: effect of membrane pre-stress. *J. Fluid Mech.* **589**, 157–181.

LI, H. & MA, G. 2010 Modelling performance of a two-dimensional capsule in a microchannel flow: long-term lateral migration. *Phys. Rev.* E **82**, 026304.

LI, X. Y. & SARKAR, K. 2005 Drop dynamics in an oscillating extensional flow at finite Reynolds numbers. *Phys. Fluids* **17**, 027103.

LI, X. Y. & SARKAR, K. 2006 Drop deformation and breakup in a vortex at finite inertia. *J. Fluid Mech.* **564**, 1–23.

LI, X. Y. & SARKAR, K. 2008 Front-tracking simulation of a liquid capsule enclosed by an elastic membrane. *J. Comput. Phys.* **227**, 4998–5018.

LORZ, B., SIMSON, R., NARDI, J. & SACKMANN, E. 2000 Weakly adhering vesicles in shear flow: tanktreading and anomalous lift force. *Europhys. Lett.* **51**, 468–474.

MUKHERJEE, S. & SARKAR, K. 2009 Effects of viscosity ratio on deformation of a viscoelastic drop in a Newtonian matrix under steady shear. *J. Non-Newtonian Fluid Mech.* **160**, 104–112.

MUKHERJEE, S. & SARKAR, K. 2010 Effects of viscoelasticity on the retraction of a sheared drop. *J. Non-Newtonian Fluid Mech.* **165**, 340–349.

MUKHERJEE, S. & SARKAR, K. 2011 Viscoelastic drop falling through a viscous medium. *Phys. Fluids* **23**, 013101.

MUKHERJEE, S. & SARKAR, K. 2013 Effects of matrix viscoelasticity on the lateral migration of a deformable drop in a wall-bounded shear. *J. Fluid Mech.* **727**, 318–345.

OLAPADE, P. O., SINGH, R. K. & SARKAR, K. 2009 Pairwise interactions between deformable drops in free shear at finite inertia. *Phys. Fluids* (21)063302.

OLLA, P. 1997*a* The lift on a tank-treading ellipsoidal cell in a shear flow. *J. De Physique Ii* **7**, 1533–1540.

OLLA, P. 1997*b* The role of tank-treading motions in the transverse migration of a spheroidal vesicle in a shear flow. *J. Phys.* A **30**, 317–329.

OLLA, P. 1999 Simplified model for red cell dynamics in small blood vessels. *Phys. Rev. Lett.* **82**, 453–456.

PRANAY, P., HENRIQUEZ-RIVERA, R. G. & GRAHAM, M. D. 2012 Depletion layer formation in suspensions of elastic capsules in Newtonian and viscoelastic fluids. *Phys. Fluids* (24)061902.

REINKE, W., GAEHTGENS, P. & JOHNSON, P. C. 1987 Blood-viscosity in small tubes: effect of shear rate, aggregation, and sedimentation. *Am. J. Physiol.* **253**, H540–H547.

ROSENKILDE, C. E. 1967 Surface-energy tensors. *J. Math. Phys.* **8**, 84–88.

SARKAR, K. & SCHOWALTER, W. R. 2000 Deformation of a two-dimensional viscoelastic drop at non-zero Reynolds number in time-periodic extensional flows. *J. Non-Newtonian Fluid Mech.* **95**, 315–342.

SARKAR, K. & SCHOWALTER, W. R. 2001 Deformation of a two-dimensional drop at non-zero Reynolds number in time-periodic extensional flows: numerical simulation. *J. Fluid Mech.* **436**, 177–206.

SARKAR, K. & SINGH, R. K. 2013 Spatial ordering due to hydrodynamic interactions between a pair of colliding drops in a confined shear. *Phys. Fluids* (25)051702.

SEIFERT, U. 1999 Hydrodynamic lift on bound vesicles. *Phys. Rev. Lett.* **83**, 876–879.

SHAPIRA, M. & HABER, S. 1990 Low Reynolds number motion of a droplet in shear flow including wall effects. *Intl J. Multiphase Flow* **16**, 305–321.

SHIN, S. J. & SUNG, H. J. 2011 Inertial migration of an elastic capsule in a Poiseuille flow. *Phys. Rev.* E **83**, 046321.

SHRIVASTAVA, S. & TANG, J. 1993 Large deformation finite-element analysis of nonlinear viscoelastic membranes with reference to thermoforming. *J. Strain Anal. Engng Design* **28**, 31–51.

SINGH, R. K. & SARKAR, K. 2009 Effects of viscosity ratio and three-dimensional positioning on hydrodynamic interactions between two viscous drops in a shear flow at finite inertia. *Phys. Fluids* (21)103303.

SINGH, R. K. & SARKAR, K. 2011 Inertial effects on the dynamics, streamline topology and interfacial stresses due to a drop in shear. *J. Fluid Mech.* **683**, 149–171.

SKALAK, R., TOZEREN, A., ZARDA, R. P. & CHIEN, S. 1973 Strain energy function of red blood-cell membranes. *Biophys. J.* **13**, 245–280.

SMART, J. R. & LEIGHTON, D. T. 1991 Measurement of the drift of a droplet due to the presence of a plane. *Phys. Fluids* A **3**, 21–28.

SUKUMARAN, S. & SEIFERT, U. 2001 Influence of shear flow on vesicles near a wall: a numerical study. *Phys. Rev.* E (64)011916.

TANGELDER, G. J., TEIRLINCK, H. C., SLAAF, D. W. & RENEMAN, R. S. 1985 Distribution of blood platelets flowing in arterioles. *Am. J. Physiol.* **248**, H318–H323.

TAYLOR, G. I. 1934 The formation of emulsions in definable fields of flow. *Proc. R. Soc. Lond. Series* A **146**, 0501–0523.

TRYGGVASON, G., BUNNER, B., ESMAEELI, A., JURIC, D., AL-RAWAHI, N., TAUBER, W., HAN, J., NAS, S. & JAN, Y. J. 2001 A front-tracking method for the computations of multiphase flow. *J. Comput. Phys.* **169**, 708–759.

UIJTTEWAAL, W. S. J. & NIJHOF, E. J. 1995 The motion of a droplet subjected to linear shear flow including the presence of a plane wall. *J. Fluid Mech.* **302**, 45–63.

UIJTTEWAAL, W. S. J., NIJHOF, E. J. & HEETHAAR, R. M. 1993 Droplet migration, deformation, and orientation in the presence of a plane wall: a numerical study compared with analytical theories. *Phys. Fluids* A **5**, 819–825.